

# Small-scale Fading for an Indoor Wireless Channel with Modulated Backscatter

Daeyoung Kim, Mary Ann Ingram, and W. Whit Smith  
Smart Antenna Research Laboratory  
School of Electrical and Computer Engineering  
Georgia Institute of Technology, Atlanta, GA 30332-0250, USA  
E-mail: {dykim, maryann.ingram, and whit.smith}@ece.gatech.edu

*Abstract*—Modulated backscatter is a RF transmission technique useful for short-range, low-data-rate applications constrained to have extremely low power requirements, such as electronic shelf tags, RF tags, and some sensor applications. The small-scale fading observed on the backscattered signal has deeper fades than a signal from a traditional one-way link of the same range in the same environment because the fading on the backscattered signal is a product of the fading on the off-board generated carrier times the fading on the reflected signal. We present the first published reports of measured cumulative distribution functions for the small-scale fading at 2.4 GHz over this type of link.

## I. INTRODUCTION

RF tags or RF transponders have been widely used in various applications, which include non-stop toll collection [1] and electronic shelf tags (ESTs) [2]. The types of RF tags are passive, semi-passive, and active. The passive and semi-passive RF tags have no RF transmitter, and many use modulated backscatter to transmit information from the RF tag to the interrogator. Their range is typically short, 2 to 30 m [3]. Because the tag has no power amplifier, passive and semi-passive tags are appropriate for low-data-rate applications that are constrained to have extremely low power requirements.

Modulated backscatter operation is illustrated in Fig. 1. The low-power transmitter is indicated as the “reflection antenna” in the figure. The RF carrier is generated off-board at Antenna 1. The terminals of the reflection antenna are switched alternately between open and closed states, thereby conveying information by modulating the reflected signal [2]. The backscattered signal is received by Antenna 2. There are also unmodulated paths between Antenna 1 and Antenna 2 in Fig. 1. Therefore, the receiver at Antenna 2 must filter out the carrier component.

There are two segments of propagation for this type of link: Antenna 1-to-reflection antenna and reflection antenna-to-Antenna 2. The two-way nature of this link means that the path loss follows  $1/d^4$ , where  $d$  is distance of one segment. The small-scale fading observed on the backscattered signal has deeper fades than a signal received over a traditional one-way link of the same range in the same environment. This happens because the fading on the backscattered signal is a product of the fades on the two segments prior to demodulation.

This paper presents measured cumulative distribution functions (CDFs) for the small-scale fading at 2.4 GHz over this type of link. One goal of this paper is to determine the theoretical distributions that best fit the measured data. Another is to ver-

This research was supported by NCR Co. Ltd. and the Georgia Tech Broadband Institute.

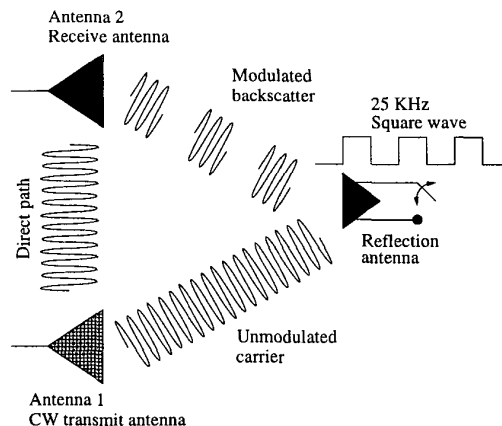


Fig. 1. Modulated backscattered signals.

ify that the modulated backscattered propagation channel can be modeled by the product of two uncorrelated one-way fades. We will first explain the measurement setup and procedure. Next the measured CDFs are compared with some theoretical CDFs using mean square error (MSE)-based goodness-of-fit tests.

## II. MEASUREMENT SETUP AND PROCEDURE

The measurements were taken in the Smart Antenna Research Laboratory at Georgia Tech, a usual small office environment with soft partitions, desks, computers, metal cabinets and bookshelves. The laboratory is located on the fifth floor of the five-story GCATT building. A partial floor plan of the fifth floor is shown in Fig. 2. Note that there is a kitchen next to the laboratory. The microwave oven in there was disabled during the measurements. The measurements were taken at night to minimize movement in the environment.

The measurement setup is shown in Fig. 3. An EST from the DecisioNet™ system [2], which serves as our reflection antenna, was modified to allow the antenna to be switched continuously by an HP33120A function generator at a rate of 25 KHz with a 50 % duty cycle. The EST was mounted on the T-shaped fixture made of plastic as shown in Fig. 4. The reflection antenna had a broad dipole-like pattern. The unmodulated RF carrier was transmitted by a patch antenna in the suspended ceiling, indicated by Antenna 1 in Fig. 3. The patch antenna had a gain of 4 dBi with an hemispherical/omni-directional pattern.

An active patch antenna, indicated by Antenna 2 in the fig-

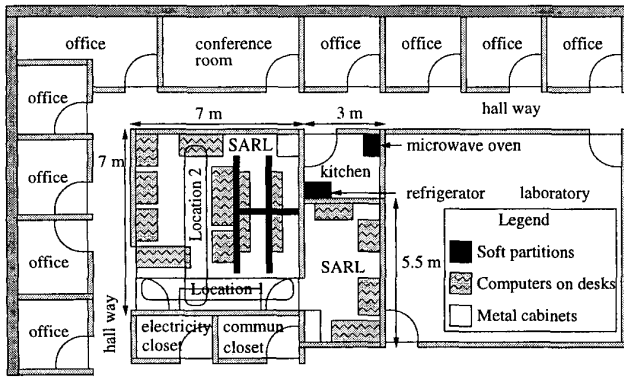


Fig. 2. A partial floor plan of the fifth floor of the GCATT building.

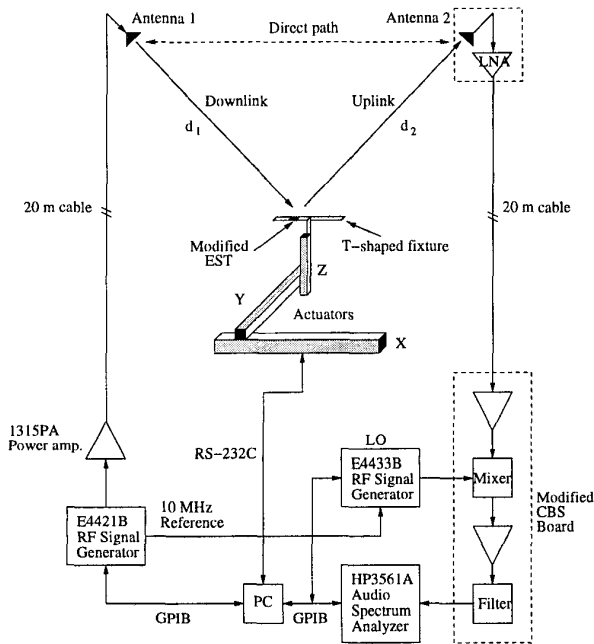


Fig. 3. The measurement setup for two-way propagation.

ure, with a pattern similar to Antenna 1, was used to receive the backscattered signal. The active antenna included the low-noise amplifier (LNA) HP INA-10386. Its output signal went to a modification of the DecisioNet™ ceiling base station (CBS), which included amplifiers, a mixer, and an 8th-order filter and which produced I and Q outputs. The local oscillator (LO) for the mixer was detuned by 1 KHz [4] to get IF conversion, and the I output at 26 KHz was monitored on an audio spectrum analyzer. A computer controlled all instruments through GPIB and RS-232C interfaces and collected data for further analysis.

To cause small-scale fading, the EST was moved in a localized volume using X, Y, and Z actuators on a moving cart, which is shown in Fig. 4. The scanning distance on X-actuator was 50 cm, which equals four  $\lambda$  at 2.4 GHz, and 400 samples were taken uniformly over its length. Therefore, the sampling interval was  $0.01 \lambda$ , or 0.125 cm, and this gave enough resolution not to miss the deepest fades. The X axis scans were repeated

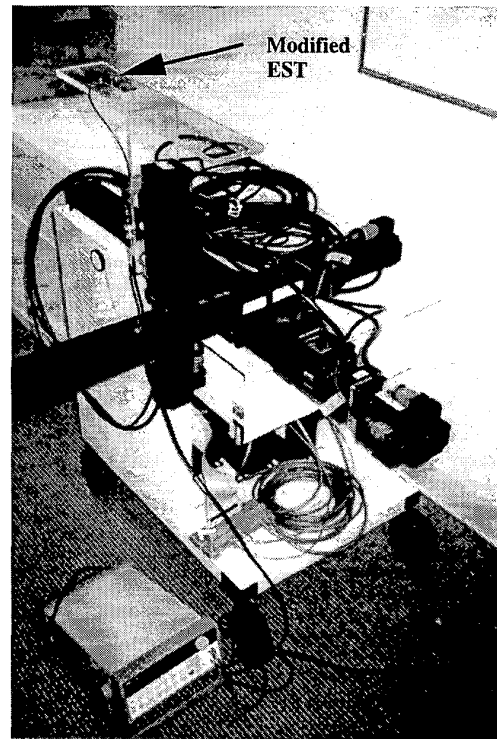


Fig. 4. The EST setup on X, Y, and Z actuators on a moving cart.

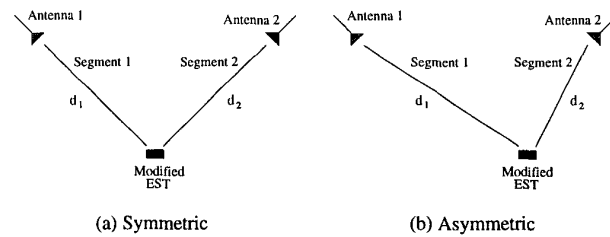


Fig. 5. a symmetric and an asymmetric geometries.

at five Y axis positions with 10 cm separations and at two Z axis positions with five cm separation. The Y and Z separations were large enough to ensure uncorrelated fading. Thus, a total of 4000 samples were taken across the volume.

To increase the sample size to improve the quality of our CDF estimates, the volume scan was repeated at 2.4, 2.44, and 2.48 GHz. The 40 MHz separation gave uncorrelated data in indoor channels [5]. Therefore, by combining volume scanning with frequency stepping, we were able to generate 12,000 samples. The data within each frequency set was normalized by its average value for the purpose of system frequency response calibration before combining the frequency sets. The data were collected at locations 1 and 2 in Fig. 2 with symmetric and asymmetric geometries. The side views of both geometries are shown in Fig. 5. For a symmetric geometry, Antennas 1 and 2 were attached to the ceiling, and the EST was placed half way between Antennas 1 and 2 as shown in Fig. 5(a). The three antennas were in a plane that was perpendicular to the ceiling. The distances on both the first and second segments of propagation, shown as  $d_1$

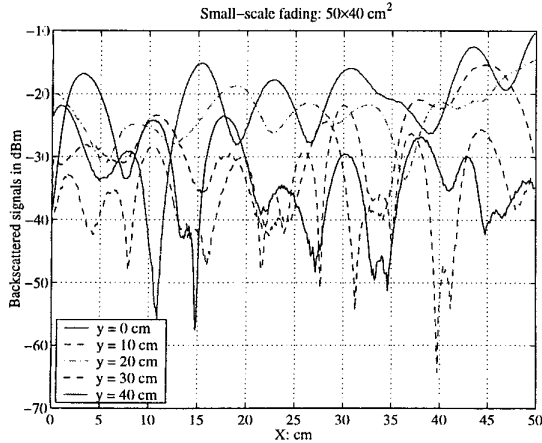


Fig. 6. The faded envelopes of five scans for Configuration 2.

and  $d_2$  in the figure, were approximately 4 m. For an asymmetric geometry, the three antennas were still in a plane perpendicular to the ceiling, but  $d_1$  and  $d_2$  were approximately 4 m and 3 m, respectively.

This paper shows the results of three measurements with the following configurations:

- Configuration 1: A symmetric geometry at location 1
- Configuration 2: A symmetric geometry at location 2
- Configuration 3: An asymmetric geometry at location 2.

For Configuration 3, the fades along individual segments and the two-way fades were measured in consecutively during 16 hours in order to confirm that the two-way fade is the product of two one-way fades. In the measurement setup for the one-way measurement, two RF signal generators, which were directly connected to two antennas, transmitted CW alternatively in time. The active antenna at Antenna 2 was replaced with the passive antenna that was Antenna 1 in Fig. 3. The modified EST in Fig. 3 was again modified to receive the faded signal continuously, and the peak amplitudes at RF frequency were captured by the RF spectrum analyzer.

### III. ANALYSIS OF THE MEASURED DATA

#### A. The Envelopes of the Faded signal

Fig. 6 shows measured data for five scans along the X actuator for one Z position and five Y positions, respectively. This faded signal was collected for Configuration 2. The horizontal axis indicates position of the EST on the X actuator and the vertical axis indicates the strength of the first harmonic of the backscattered signal in dBm. A maximum fading variation of 54 dB is observed for this system configuration, which features line-of-sight (LOS) for both propagation segments. The deep nulls in some of the scans may be explained by strong reflections from metal bookshelves near the EST.

#### B. The Measured CDFs

The CDFs of the measured data for the three configurations are compared with three theoretical CDFs: “XYRician”, Nakagami and log-normal. “XYRician” is the CDF for the product of two independent Rician random variables with the same

$K$  values. When the CDFs of the Rician and the XYRician are computed, the amplitude of the specular component is set to one for simplicity [6]. The XYRician distribution is considered because of the product form of the fading for modulated backscatter. The comparisons are made graphically and in terms of four different metrics that are based on the MSE between the measured and theoretical CDFs.

The number of samples on the X-axis is 400. Since two samples separated by  $0.5 \lambda$  are considered uncorrelated [7], there are approximately 10 uncorrelated samples on the X-axis. Therefore, a total of 300 uncorrelated samples are among the 12,000 samples. According to the Kolmogorov-Smirnov two-sided test, the measured distribution is within  $\pm 7\%$  of the true distributions with 10% level of significance [8][9].

In computing the average probability of error for data transmission over a fading channel, the probability density function of the faded envelopes is used to average the conditional probability of error at each envelope level. The weak signal envelope heavily influences the average probability of error [5]. To take this into consideration in curve fitting, the log of the CDF is considered in addition to the CDF. A second way we can emphasize the smaller CDF values is to calculate the MSE only for signal levels below the median [5], which is called “half scale” in this paper. The modified MSEs for the full and half scales are computed by

$$\text{FMSE} = \frac{\sum_{x=-30}^{10} [\log_{10} F_n(x) - \log_{10} F(x)]^2}{N_{full}} \quad (1)$$

$$\text{HMSE} = \frac{\sum_{x=-30}^0 [\log_{10} F_n(x) - \log_{10} F(x)]^2}{N_{half}}, \quad (2)$$

respectively. The values of the index  $x$  are signal powers relative to the median, incremented in 1 dB steps.  $F_n(x)$  is a measured CDF, and  $F(x)$  is a theoretical CDF.  $N_{full}$  and  $N_{half}$ , which are 41 and 31, are the numbers of bins for the full and half scales, respectively. The MSEs computed on the linear scale are the same as in (1) and (2) except the logarithms are not taken. The various MSEs for each configuration are shown in Table I.

A couple of general comments about the table are helpful in its interpretation. First, the position of the boldface value indicates the particular metric that was used to optimize the parameter of the CDF. For example, for Configuration 1, 0.66 is the value of  $m$  that yields the best fit of the Nakagami distribution when the linear, full scale is used. Second, we observe that use of the log scale weights the smaller values of the CDF so heavily that the choice of half or full scale becomes irrelevant.

Of the three theoretical distributions considered, the XYRician has the best fit for 10 of the 12 combinations of metrics and configurations. The two exceptions are that log-normal is preferred for Configurations 1 and 3 when the linear, half-scale is used. In the 10 combinations for which the XYRician is the best fit, the Nakagami and log-normal are tied for the next best fit. The optimal  $K$  parameter for the XYRician varies between  $-10$  dB and  $0$  dB for all combinations of metrics and configurations, however, we note that there is very little difference between the CDFs for these values, especially between  $-10$  dB

TABLE I  
FOUR MSE-BASED METRICS OF THE CDFs FOR THREE CONFIGURATIONS.

Configuration	CDF	Full scale			Half scale		
		Parameter	Log scale	Linear scale	Parameter	Log scale	Linear scale
1	XYRician; $K$	-10 dB	$1.90 \times 10^{-3}$	$2.24 \times 10^{-4}$	-10 dB	$2.56 \times 10^{-3}$	$1.88 \times 10^{-4}$
		-10 dB	$1.90 \times 10^{-3}$	$2.24 \times 10^{-4}$	-10 dB	$2.56 \times 10^{-3}$	$1.88 \times 10^{-4}$
	Nakagami; $m$	0.72	$5.95 \times 10^{-3}$	$1.61 \times 10^{-3}$	0.72	$7.73 \times 10^{-3}$	$6.01 \times 10^{-4}$
		0.66	$1.20 \times 10^{-2}$	$1.08 \times 10^{-3}$	0.59	$4.94 \times 10^{-2}$	$1.17 \times 10^{-4}$
	Log-normal; $\sigma$	10.5 dB	$3.90 \times 10^{-3}$	$1.55 \times 10^{-3}$	10.5 dB	$4.74 \times 10^{-3}$	$2.53 \times 10^{-4}$
		8.5 dB	$1.76 \times 10^{-1}$	$5.42 \times 10^{-4}$	9.5 dB	$4.67 \times 10^{-2}$	$4.30 \times 10^{-5}$
2	XYRician; $K$	-5 dB	$6.75 \times 10^{-4}$	$8.57 \times 10^{-6}$	-5 dB	$9.21 \times 10^{-4}$	$7.41 \times 10^{-6}$
		-5 dB	$6.75 \times 10^{-4}$	$8.57 \times 10^{-6}$	-7 dB	$9.48 \times 10^{-4}$	$6.88 \times 10^{-6}$
	Nakagami; $m$	0.74	$1.32 \times 10^{-3}$	$8.31 \times 10^{-4}$	0.74	$1.56 \times 10^{-3}$	$1.97 \times 10^{-4}$
		0.60	$3.74 \times 10^{-2}$	$3.23 \times 10^{-4}$	0.66	$1.74 \times 10^{-2}$	$6.18 \times 10^{-5}$
	Log-normal; $\sigma$	10.3 dB	$1.34 \times 10^{-2}$	$2.55 \times 10^{-3}$	10.3 dB	$1.75 \times 10^{-2}$	$7.24 \times 10^{-4}$
		7.6 dB	$4.90 \times 10^{-1}$	$5.26 \times 10^{-4}$	8.6 dB	$2.01 \times 10^{-1}$	$6.08 \times 10^{-5}$
3	XYRician; $K$	0 dB	$2.33 \times 10^{-3}$	$4.24 \times 10^{-4}$	0 dB	$3.10 \times 10^{-3}$	$2.39 \times 10^{-4}$
		-10 dB	$6.09 \times 10^{-3}$	$5.28 \times 10^{-5}$	-10 dB	$8.31 \times 10^{-3}$	$5.84 \times 10^{-5}$
	Nakagami; $m$	0.78	$3.69 \times 10^{-3}$	$1.05 \times 10^{-3}$	0.78	$4.64 \times 10^{-3}$	$5.57 \times 10^{-4}$
		0.58	$7.95 \times 10^{-2}$	$4.94 \times 10^{-4}$	0.65	$4.85 \times 10^{-2}$	$1.76 \times 10^{-4}$
	Log-normal; $\sigma$	10.0 dB	$1.64 \times 10^{-2}$	$1.74 \times 10^{-3}$	10.0 dB	$2.18 \times 10^{-2}$	$3.63 \times 10^{-4}$
		7.9 dB	$2.91 \times 10^{-1}$	$4.46 \times 10^{-4}$	8.8 dB	$1.12 \times 10^{-1}$	$1.23 \times 10^{-5}$

and -5 dB. The low values of  $K$  for these LOS configurations may be explained by strong reflections from nearby metal cabinets and bookshelves.

The measured CDFs for the sample sets of Configurations 1 and 2 are plotted with symbols in Figs. 7 and 8, respectively, along with the best fitting theoretical CDFs (in terms of MSE of the logs of the CDFs). All CDFs are normalized to the median level for convenient comparison. The Rayleigh and Rician with  $K = 6$  dB distributions are also shown in the figures as a reference.

The measured CDFs show that two-way fading is more severe than traditional one-way fading. For example, in Fig. 7, the two-way fade at the 1 % level (i.e. at probability =  $10^{-2}$ ) is 6 dB lower than the fade at the 1 % level for the Rayleigh distribution. This means that the fade margin for a modulated backscatter link to ensure 99 % availability would be 6 dB larger than the fade margin for a one-way Rayleigh faded link with the same median path loss.

Fig. 9 compares the measured CDF for Configurations 1 and 2. The tail parts of the measured CDFs are very similar, but the middle parts are slightly different. The different cluttering environment between Configurations 1 and 2 may explain this CDF discrepancy. Location 2 is relatively open compared to location 1. In location 1, there are metal bookshelves alongside the actuator setup. The MSEs between the logs of the measured CDFs are  $3.85 \times 10^{-3}$  and  $5.22 \times 10^{-3}$  for the full and half scales, respectively.

To further investigate the product-based model of the fading, the fading distributions for the individual segments were determined and the CDF of the product of these fades was compared

to the measured two-way CDF and various theoretical CDFs. For this study, Configuration 3 was used, which corresponds to the asymmetric geometry in Fig. 5(b). The CDFs are shown in Fig. 10. The CDF of each segment is close to the Rayleigh distribution in spite of the presence of LOS on both branches of propagation. This may be explained relatively strong reflections from metal cabinets and bookshelves.

The correlation coefficient  $\rho_{XY}$  of the one-way fades was found as follows. Let  $X$  and  $Y$  be  $N \times 1$  column vectors of fade samples such that their  $i$ th elements,  $x_i$  and  $y_i$ , are the measured envelopes at the carrier frequency for the first and second segments, respectively, when the tag is in the  $i$ th position. Then

$$\rho_{XY} = \frac{(1/N)X^T Y - \bar{X}\bar{Y}}{\bar{\sigma}_X \bar{\sigma}_Y}, \quad (3)$$

where  $\bar{X}$  and  $\bar{Y}$  are sample means and  $\bar{\sigma}_X^2$  and  $\bar{\sigma}_Y^2$  sample variances. For  $N = 12,000$  samples,  $\rho_{XY} = 0.043$ , indicating almost no correlation in the fades of the segments.

The CDF of the measured two-way fades is within  $7.67 \times 10^{-3}$  of the CDF of the product of measured one-way fades in terms of log, full scale MSE, and within  $1.05 \times 10^{-2}$  in terms of log, half scale MSE. These MSE values as well as the plot indicate a fairly good agreement between the two sets of data. The small differences may be explained by the fact that one of the ceiling antennas was exchanged with another similar one for the one-way measurement and the other ceiling antenna may have been moved slightly when connections were changed.

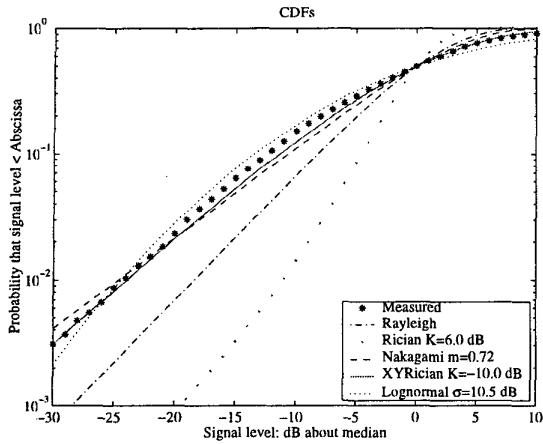


Fig. 7. The measured CDF for Configuration 1.

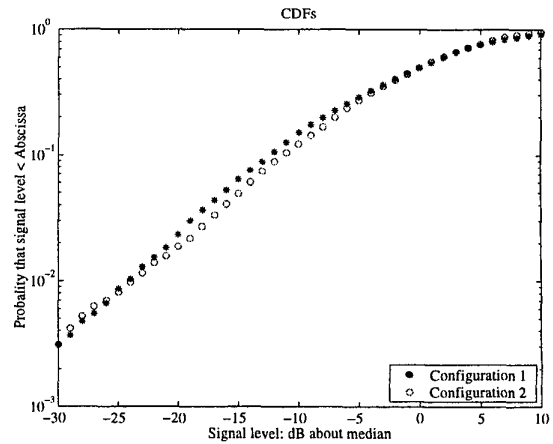


Fig. 9. The measured CDFs for Configurations 1 and 2

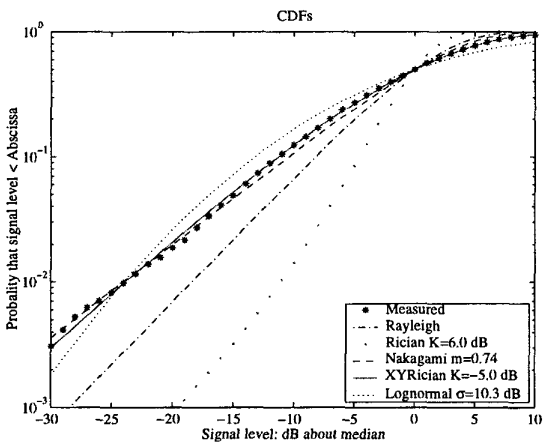


Fig. 8. The measured CDF for Configuration 2.

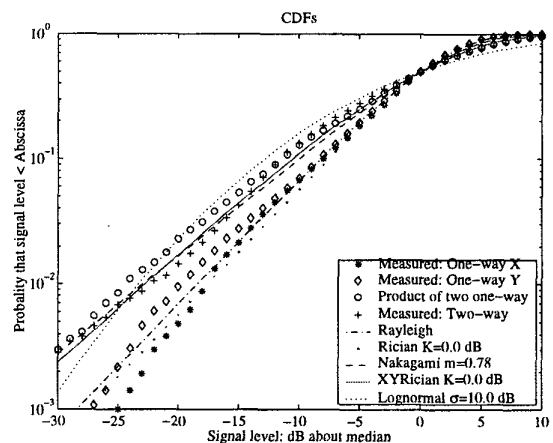


Fig. 10. The measured CDFs for Configuration 3.

#### IV. CONCLUSIONS

Small-scale fading statistics for modulated backscatter in an indoor, small office environment at 2.4 GHz have been presented. These statistics show significantly deep fades in spite of the presence of LOS on both segments of propagation. The results suggest that the small-scale fading on a modulated backscatter link can be modeled by a product of independent Rician random variables or by a Nakagami random variables.

#### ACKNOWLEDGMENTS

The authors would like to thank Dr. Albert Claessen of NCR for his helpful suggestions in the course of this work.

#### REFERENCES

- [1] P. Blythe, "RFID for road tolling, road-use pricing and vehicle access control," in *IEE Colloquium on RFID Technol.*, pp. 8/1–8/16, Oct. 1999.
- [2] J. G. Evans, R. A. Shober, S. A. Wilkus, and G. A. Wright, "A low-cost radio for an electronic price label system," *Bell Labs Tech. J.*, pp. 203–215, Autumn 1996.
- [3] J. R. Tuttle, "Traditional and emerging technologies and applications in the radio frequency identification (RFID) industry," in *IEEE Radio Freq. Integrated Circuits Symp.*, pp. 5–8, June 1997.
- [4] M. Kossel, H. R. Benedickter, R. Peter, and W. Bächtold, "Microwave backscatter modulation systems," in *IEEE MTT-S Int. Microwave Symp. Digest*, vol. 3, pp. 1427–1430, June 2000.

- [5] K. Pahlavan and A. H. Levesque, *Wireless Information Networks*. Chichester: John Wiley & Sons, 1995.
- [6] T. S. Rappaport and C. D. McGillem, "UHF fading in factories," *IEEE J. Select. Areas Commun.*, vol. 7, pp. 40–48, Jan. 1989.
- [7] W. C. Jakes, *Microwave Mobile Communications*. New York: IEEE Press, 1993.
- [8] D. Zwillinger, *Standard Mathematical Tables and Formulae*. Boca Raton: CRC Press, 30th ed., 1996.
- [9] H. Hashemi, M. McGuire, and T. Vlasschaert, "Measurements and modeling of temporal variations of the indoor radio propagation channel," *IEEE Trans. Veh. Technol.*, vol. 43, pp. 733–737, Aug. 1994.